A Compact Hybrid Silicon/Electro-Optic Polymer Resonant Cavity Modulator Design

K. K. McLauchlan and S. T. Dunham
Electrical Engineering Department, University of Washington, Seattle, WA, USA 98195-2500;

ABSTRACT

The design and simulation of a novel resonant cavity optical modulator incorporating a hybrid silicon/electro-optic polymer slot waveguide structure is presented in this work. The device utilizes the electro-optic polymer in the cavity region to provide an active material for modulation and includes distributed Bragg reflectors in single mode silicon waveguide regions at each end of the cavity to create a narrow response peak at the resonant wavelength. Simulation results show that this electro-optic modulator design can simultaneously attain a large modulation depth, short device length and a low drive voltage, all of which are expected to be necessary for future high speed integrated optics devices. The high operating frequency and complex nature of the structure lead to a need for full 3D simulations in order to obtain accurate propagation characteristics, particularly concerning scattering losses. However, 3D simulations are very computationally expensive, especially during design optimization. Therefore, the periodicity of the device has been exploited to allow a cascade matrix approach to be employed to reduce the necessary computational resources required for accurate simulation of the propagation characteristics. The design and fabrication process have been chosen to allow for the majority of the fabrication to be completed before the electro-optic polymer is introduced into the process, which enables the use of well-established CMOS processing techniques, and should accelerate the transition to hybrid silicon/electro-optic polymer devices in future integrated optics applications.

Keywords: Optical modulation, Electro-optic polymer, Integrated optics, Silicon photonics

1. INTRODUCTION

There has been an increasing interest in high-density integrated optics in recent years. One of the more promising ways of achieving this is through the use of silicon-on-insulator (SOI) wafers, which are also CMOS compatible, thereby allowing for the use of the well-established processing methods for silicon. In order to realize fully integrated optics, all optical components must be not only CMOS compatible, but also have small dimensions and excellent operational characteristics. Optical modulators are one component in which it is challenging to simultaneously achieve small size along with a strong, high-speed response in silicon devices. The V_π-L product, which combines the length of the active region with the voltage necessary to achieve a phase shift of π radians, is a common figure of merit for Mach-Zehnder (MZ) modulator structures. A silicon MZ modulator has been demonstrated that exhibits a 1GHz modulation bandwidth, but the V_π-L product is still 8V-cm [1]. A Fabry-Perot (FP) resonant cavity device in SOI has been demonstrated that is less than 20µm in length, but an applied voltage of 3.7V only resulted in a modulation depth of the transmitted intensity of 53% [2], which may not be sufficient for accurate detection of modulation. A MZ modulator demonstrated with an electro-optic (EO) polymer exhibited a V_π-L product of 2.2V-cm, which is even better than lithium niobate MZ modulators, which are the current industry standard [3]. An EO polymer/silicon microring resonator has been demonstrated that combines the benefits of both silicon and the fast, strong response of EO polymers. This structure has a ring radius of 100µm and required an applied voltage of 20V in order to change the output intensity by 5dB [4]. Recent advances in the design of EO polymers have resulted in polymers with both a fast response and very large EO coefficients, which allow for the fast switching with low applied voltages that will be necessary for integrated optics applications. These EO polymers should allow for excellent operational characteristics in an optical modulator, but due to the relatively low index of refraction of the polymers, device footprints are generally quite large and EO polymers are not CMOS compatible for integrated applications. The structure proposed here combines the benefits of both silicon and EO polymers to create a high-speed device with a large modulation depth, low drive voltage, and very compact size that allows all of the silicon processing to be completed using standard CMOS processing before the EO polymer is introduced into the structure.

Tuning the Optic Response of Photonic Bandgap Structures III, edited by Paul V. Braun, Sharon M. Weiss,
Proc. of SPIE Vol. 6322, 632203, (2006) · 0277-786X/06/$15 · doi: 10.1117/12.679128

2. RESONANT CAVITY MODULATOR STRUCTURE

This resonant cavity modulator design incorporates a set of distributed Bragg reflectors on each side of a hybrid slot waveguide cavity. The series of Bragg reflectors are created with circular holes appropriately spaced in a single-mode silicon waveguide to increase the reflectivity on each side of the resonant cavity, as illustrated in Fig. 1. The resonant cavity breaks the periodicity of the Bragg reflector and results in a sharp transmission peak at the resonant wavelength, determined by the length of the cavity region. The slot waveguide in the cavity region guides light in the narrow lower index of refraction region between two higher index regions, in this case silicon ridges [5]. The slot waveguide is considered 'hybrid' as it incorporates an EO polymer as the low index material in which the light will be guided. Because light is confined primarily to the EO polymer, as shown in Fig. 2, applying an electric field across the polymer will change its index of refraction. The strength of this response will depend upon the material characteristics of the EO polymer, the applied field during device operation, as well as the success of the poling process during fabrication, which aligns the chromophores in the polymer and allows for the index change. Since the silicon ridges can also serve as electrodes, the hybrid slot waveguide structure should allow for high-speed modulation will small applied voltages.

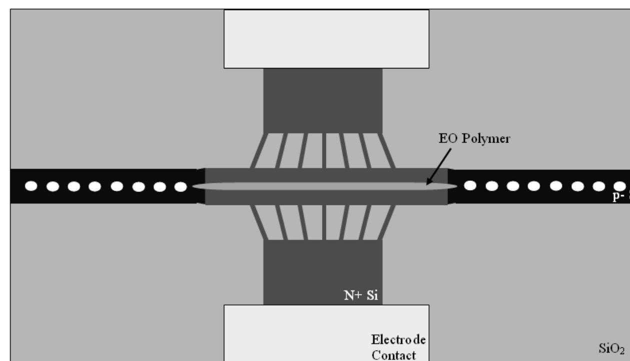

Fig. 1. Top view of the hybrid silicon/electro-optic polymer resonant cavity modulator. The total length of the device is less than 30μm, and the bulk of the processing can be completed using standard CMOS fabrication techniques.

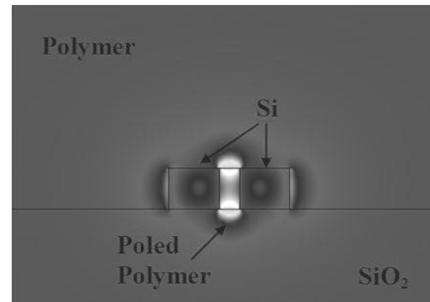

Fig. 2. Cross-section of a finite element simulation of the hybrid slot waveguide structure showing the field confinement in the low index EO polymer region rather than the higher index silicon ridges.

For the design of this device, the dimensions of the hybrid waveguide were optimized to achieve the largest change in the propagation constant, as shown in Fig. 3. This change in propagation constant, $\Delta\beta$, is determined for a given index of refraction of the EO polymer (n = 1.6 at λ = 1.55μm) and an assumed EO coefficient for the poled polymer (r_{33} = 100pm/V) with Eq. 1 shown below:

$$\Delta\beta = \beta_1 - \beta_2 = \frac{2\pi}{\lambda_0}(n_1 - n_2) \qquad (1)$$

where λ_0 is the wavelength in free space, n_1 is the index of refraction with no applied voltage, and n_2 is the index of refraction with an applied voltage, V_a, and electrode spacing, w_{eo}, as given by

$$n_2 = n_1 - \frac{n_1^3 r_{33} V_a}{2 w_{eo}} \qquad (2)$$

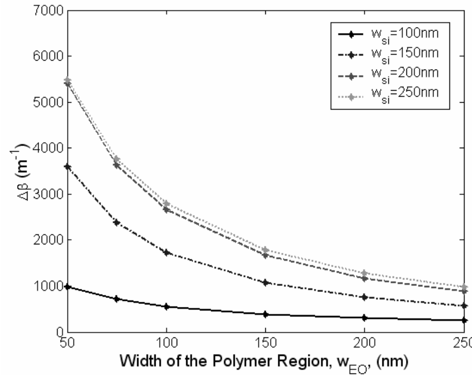

Fig. 3. The change in propagation constant calculated from finite element simulations showing that there is a larger change in propagation constant for a given applied voltage as the width of the polymer region is reduced and that the width of the silicon ridges should be wide enough to promote confinement of the field in the polymer, but not large enough to strongly confine a guided mode individually.

The hybrid slot waveguide structure reduces the necessary applied voltage for a given change in propagation constant since the silicon ridges, which are necessary to facilitate guiding of light in the low index polymer, also act as electrodes. The resulting electrode spacing is significantly reduced from that required for an all-polymer waveguide, where the electrodes must be placed sufficiently far away from the waveguide to prevent excessive propagation loss. Also illustrated in Fig. 3, as the minimum feature size in modern CMOS fabrication facilities continues to decrease, the dimensions of the EO polymer slot in the hybrid waveguide can also be decreased, which will allow for a lower operating voltage to achieve a similar change in propagation constant and therefore the resonant wavelength.

3. SIMULATION

3.1 Simulation Method

A cascade matrix method has been employed to allow for finite element modeling of large 3D structures, which is generally very difficult due to the significant computational resources/time required to perform the full 3D analysis. With the cascade matrix method, individual sections of the device are each simulated separately, and the propagation characteristics, ***T***, of each section are then used to build up the entire device, as shown in Eq. 3 and Fig. 4 [6]. With this method, a fast 3D analysis of a 50µm structure, which would be infeasible for a full 3D finite element simulation, can be completed in less than two hours. The resonant cavity modulator structure lends itself well to the cascade method due to the periodicity of the device. As shown below, there are only four unique sections that need to be analyzed to determine the transmission characteristics of the device. This also allows for very fast design variation and optimization, as a change in the structure requires only a single section be simulated again, rather than the entire device.

$$\vec{T}_{tot} = \vec{T}_g \vec{T}_d \vec{T}_d \vec{T}_d \vec{T}_d \vec{T}_t \vec{T}_c \vec{T}_c \vec{T}_c \vec{T}_c \vec{T}_t \vec{T}_d \vec{T}_d \vec{T}_d \vec{T}_d \vec{T}_g \qquad (3)$$

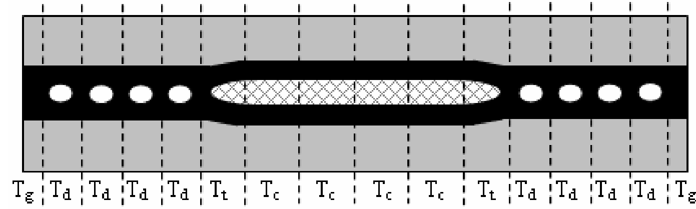

Fig. 4. Individual sections used for finite element simulations of the structure. Due to the periodicity of the device, only four unique simulations were required.

A comparison of the simulation results of a manageable section of the Bragg reflector is shown below. As the figure illustrates, there is excellent agreement between the cascade matrix method and the full finite element simulation, which required more than 7 hours to complete, while the individual sections required approximately 15 minutes each.

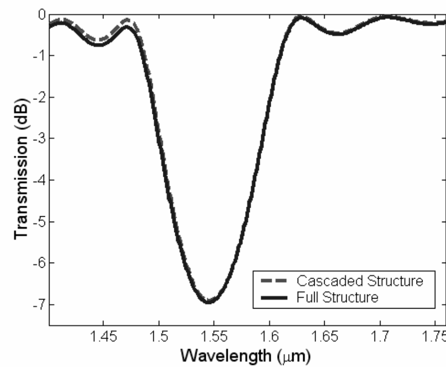

Fig. 5. A comparison of the simulations for a 7-period Bragg reflector illustrate excellent agreement between the full simulation and cascade structure.

3.2 Analysis of the simulation results of an ideal structure

The figures of merit for this device include the achievable modulation depth, which relates the difference between the outputs at the detection wavelength with and without an applied field, the full-width at half maximum (FHWM), the maximum transmission (the throughput at the resonant wavelength), and the overall length of the device. There is a general trade-off between the cavity length and the modulation depth, which limits the minimum size of the device for a given applied voltage. This relationship is illustrated in Fig. 6a, where the modulation depth increases with both increasing cavity length and number of periods in the Bragg reflector.

Increasing the number of periods in the Bragg reflector increases the modulation depth and decreases the FWHM up to a saturation point because each additional period not only increases the reflectivity, but it also adds loss to the system, which significantly reduces the transmission at the resonant wavelength. This transmission limit will be determined by the detection capabilities of the system for a given application, which will limit the number of reflector periods that can be included in the system, as shown in Fig 6b. Reducing the size of the holes in the Bragg reflector potentially increases the cost of fabrication, but also improves through-put up to the point where the difference in scattering loss between the two diameters becomes negligible for a given waveguide structure, as is also illustrated in Fig. 6b for hole diameters of 100nm and 75nm in a 600nm silicon waveguide.

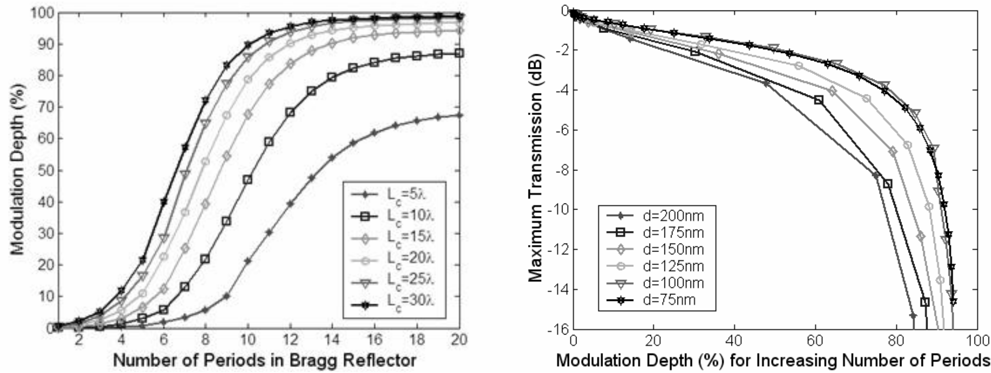

Fig. 6. Figure 6a demonstrates the increase in achievable modulation depth for a given hole diameter (100nm) as the cavity length and number of periods are increased. Figure 6b illustrates the limits to improved performance by comparing the trade-offs between throughput and modulation depth for various hole diameters.

Increasing the applied voltage also increases the change in propagation constant in the hybrid slot waveguide, and is therefore an alternative method of increasing the modulation depth. Analysis of the product of the voltage necessary to achieve a given modulation depth compared to the length of the cavity, the V_{MD}-L product, shows that the strength of each approach is similar, which leaves flexibility in design choices depending upon the desired application.

4. FABRICATION

The resonant cavity modulator design has been created to allow for the majority of the processing to be completed with standard CMOS fabrication techniques in order to facilitate the transition to organic polymer devices. Therefore the entire silicon portion of the device is fabricated before the EO polymer is introduced into the structure. Also, due to the small critical dimensions, the silicon portions of the waveguide, Bragg grating, and slot waveguide cavity region must all be defined in a single lithography and etch step, as alignment at this scale would be extremely difficult. In the experimental demonstration electron-beam lithography will be used; however, the minimum feature size has been kept large enough to allow for the entire device to be fabricated using modern CMOS technologies. Variations can also be expected to occur during the fabrication process, including variations of the doping concentrations, dimensions of the structure, filling of the cavity slot with the EO polymer, and etching sidewall roughness. The effects of each of these variations on device performance are considered in the following sections.

4.1 Doping concentration variation

The variation of the concentration of the doped silicon ridges is not expected to significantly vary the performance of the device. The desired doping concentration of $10^{18}cm^{-3}$ has been chosen so that there is not an appreciable optical loss due to propagation in the heavily doped ridges as shown in Fig. 7 below, and a change of +/- 5% will not significantly change the propagation of light in the ridges. The electrical characteristics will also vary slightly due to the variation in doping concentration, but the 3% variation in the resulting time constant due to the doping variations will not significantly change the device operation.

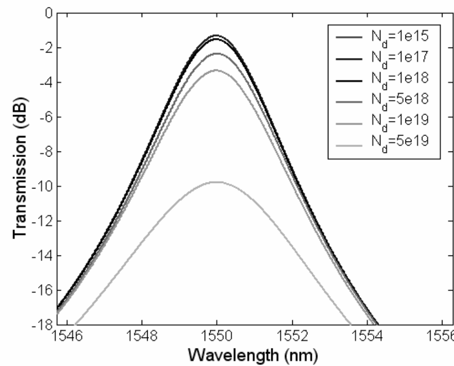

Fig. 7. Transmission response for various doping concentrations in the silicon regions of the slot waveguide cavity. Since the variation is small for doping concentrations up to $10^{18}cm^{-3}$, this is expected have little effect on modulator operation.

4.2 Size variation

There may be global variations in the dimensions of the waveguides due to the tolerances of the fabrication process, which is assumed to have a minimum line width of 100nm +/- 10%. These variations in dimensions will affect the reflectivity of the mirrors in the Bragg grating regions, as well as the active section of the hybrid slot waveguide. Fabrication variations that cause the width of the polymer region to be increased will result in a slightly lower change in propagation constant for a given applied voltage, and a reduction in the width will actually slightly increase the change in propagation constant and improve the modulation depth. However, it is the variation in the diameter of the holes in the Bragg grating, which affects the reflectivity of the mirrors for a given number of periods, that will have the most significant impact on device operation. Variations of dimension that result in the full 10% over-exposure will both increase the size of the holes in the Bragg reflector and decrease the width of the waveguide and therefore increase the reflectivity for a given number of periods and shift the resonant wavelength by 3nm. However, under-exposure of the structure will reduce the reflectivity of the Bragg grating, as each hole will have a smaller effect, as illustrated in Fig. 8 for a hole diameter for 100nm, although this effect could be reduced by increasing the length of the cavity region. Therefore the dimensions of the holes in the Bragg reflector should be chosen so that variations in size result in a tolerable change in the modulation depth and transmission for the chosen cavity length.

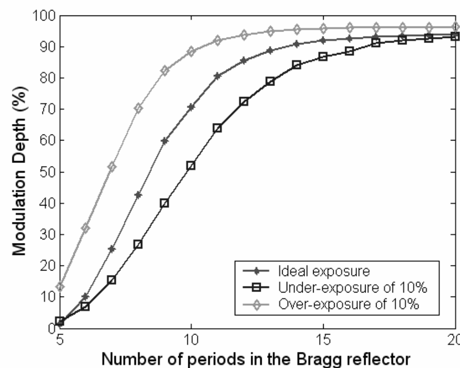

Fig. 8. The modulation depth for a structure with a 15µm cavity length and structure dimensions varying up to $\pm$10% of the minimum linewidth (100nm). Under-exposure both decreases the diameter of the holes in the Bragg reflector and increases the waveguide width, which significantly reduces the achievable modulation depth for a given applied voltage.

Local differences due to small exposure and/or etching variations may also result in the waveguide dimensions varying within a single structure. These variations are expected to be less than the global variations and will have little effect on

the hybrid slot waveguide cavity region, but will have a somewhat more significant impact on the transmission characteristics in the reflector regions as it will slightly change the hole spacing and the amount each hole will contribute to the reflectivity. Fig. 9 shows the modulation depth for a Bragg reflector composed of hole diameters randomly varied by up to +/-2%, and demonstrates that these local random variations will have very little effect on the transmission characteristics of the device.

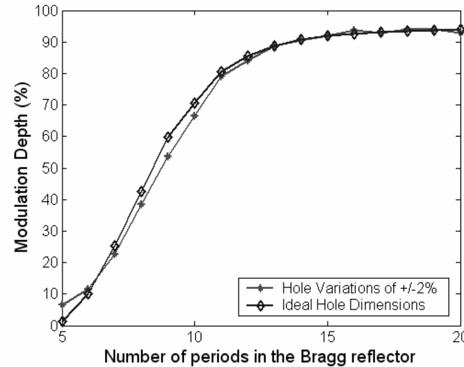

Fig. 9. The modulation depth for random variations in hole diameter of +/-2%. These variations do not significantly change the transmission characteristics of the device.

4.3 Polymer filling variation

Filling of the cavity during polymer processing is expected to be a crucial step in the fabrication process, as the achievable change in propagation constant will depend on the ability of the polymer within the slot to be poled. If there is poor filling of the slot with the polymer during fabrication, there will be less active material available during operation. The reduction of the EO polymer in the slot will reduce the change in index of refraction with an applied field, and therefore change the corresponding output by reducing the modulation depth or requiring a much larger operating voltage to achieve a similar response.

Compounding the reduction in the change in index of refraction of the EO polymer is increased loss due to reflection at the point of coupling into the hybrid slot waveguide. Because the index of refraction of the unfilled slot is lower than the index of refraction of the EO polymer, the reflection at the boundary will be greater for the slot that has less polymer filling. Due to the increased loss and reduction of the change in propagation constant, there is a significant degradation in the achievable modulation depth for a given applied voltage for the lower filling of the slot, as illustrated in Fig. 10. Therefore, the properties of the particular polymer chosen for an application will need to be investigated to verify that sufficient slot filling is achievable, as this is expected to have the most significant impact on device operation.

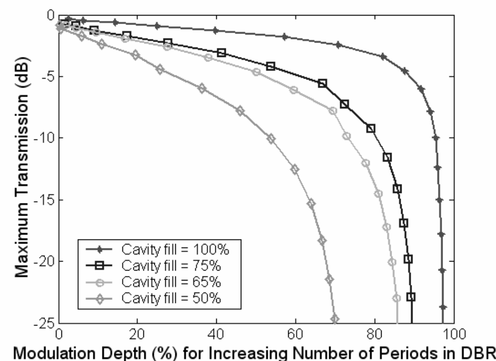

Fig. 10. Maximum transmission versus the modulation depth for various percentages of filling of the EO polymer in the slot of the hybrid waveguide. The polymer filling will be an important factor to consider during the fabrication process, as poor filling can significantly affect the operational characteristics.

4.4 Sidewall shape and surface roughness variations

The angle and roughness of the sidewalls of the silicon waveguide will likely affect the insertion loss and modulation depth of the device and may also facilitate coupling into higher order modes and/or substrate radiation modes. An estimate of acceptable sidewall roughness has been calculated according to Payne and Lacey [7]. Using this estimation, assuming a Gaussian autocorrelation function and the worst-case correlation length, the sidewall roughness must be limited to 8nm in order to avoid high propagation losses. Fabrication of the silicon waveguide will be done with a dry etch process, similar to those commonly found in CMOS fabrication facilities, as a design goal for this device was the ability to manufacture it and incorporate it into future highly integrated optics applications. It is expected that a surface roughness of less than 2nm and a sidewall angle of ~90° should be achievable in these circumstances, as the IBM photonics research group has previously demonstrated this [8]. However, with the fabrication facilities available at the Washington Technology Center (WTC), which is the facility that will be used for fabrication of the experimental structure, both sidewall angle and roughness are expected to be an issue.

The reactive ion etching system available at the WTC is a Trion Phantom Reactive Ion Etcher (RIE) with O_2, SF_6, and CHF_3 gases. Legtenberg, et al. have done an extensive study on the etching of silicon with these gases and considered the effects of various gas mixtures, RF power and pressure, and these results were used as a starting point for determining the etch chemistry for the silicon waveguide of the resonant cavity modulator [9]. Relatively good anisotropy and smooth etch surface were achieved for silicon structures etched in the Trion Phantom RIE system with SF_6 at 30sccm, O_2 at 10sccm, CHF_3 at 12sccm, RF power of 100W and a chamber pressure of 100mbar.

However, the initial sidewall roughness was too large to prevent considerable propagation losses in the waveguide. Therefore, a sidewall smoothing procedure will need to be employed in the experimental fabrication process to reduce the roughness of the reactive ion etch. Two methods have been reported that have significantly reduced the sidewall roughness of silicon waveguides: wet oxidation at 1000°C [10] and wet chemical smoothing [11]. Wet oxidation resulted in a lower propagation loss, but the process does not allow for the precise control of waveguide dimensions that is necessary for this resonant cavity modulator. Therefore the wet chemical RCA smoothing process proposed by Sparacin et al. will be used [11]. The CMOS-compatible RCA process involves a series of oxidation and oxide stripping using short dips in SC1, a dilute HF solution, and SC2. The SC1 dip acts to remove organics from the surface by trapping them in an oxide. The HF dip then removes this oxide and leaves an H-terminated silicon surface. Finally the SC2 removes any metals from the surface and creates a protective oxide. Fig. 11 shows the results of the process, which illustrates smoothing of the sidewall surface, and this should be further enhanced with the improved structure definition using electron beam lithography.

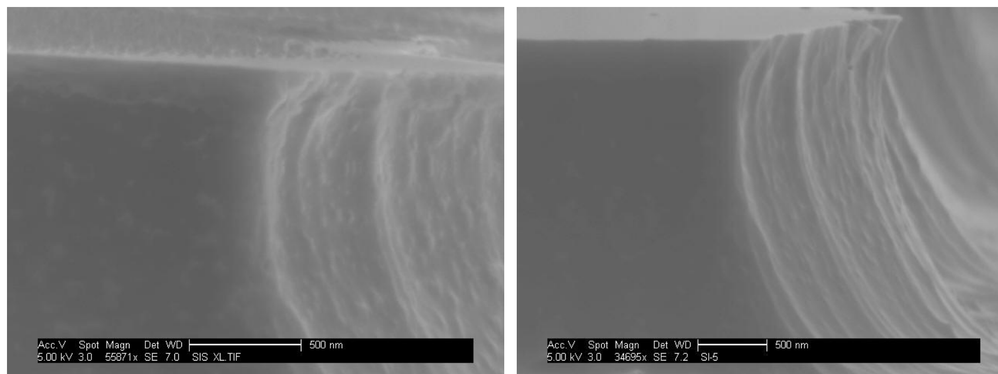

Fig. 11. Initial sidewall roughness from RIE etch process is shown in Fig. 11a (left). Fig 11b (right) shows the sidewalls after the RCA smoothing process and illustrates the improvement in the sidewall roughness.

5. CONCLUSION

The design presented in this work simultaneously provides a short device length, small applied voltages, and a fast response time using a standard CMOS processing technique for the majority of the fabrication process and finally incorporating the EO polymer in order to take advantage of its fast, strong response. The design has been analyzed using a cascade matrix method of finite element simulations, which easily incorporate design changes and allows for fast, accurate design optimization. Analysis has also shown that this structure can be designed to be robust enough to overcome the fabrication tolerances that can be expected in a CMOS process. The use of the SOI wafer and standard processing should provide a useful optical modulator for use in future integrated optics applications.

ACKNOWLEDGMENTS

Research support is gratefully acknowledged from a National Science Foundation Graduate Research Fellowship and the National Science Foundation Center on Materials and Devices for Information Technology Research (CMDITR), DMR-0120967.

REFERENCES

1. Liu, R. Jones, L. Liao, D. Samara-Rubio, D. Rubin, O. Cohen, R. Nicolaescu, and M. Paniccla, “A high-speed silicon optical modulator based on a metal-oxide-semiconductor capacitor,” *Nature*, vol. 427, pp. 615-618, Feb. 2004.
2. C. A. Barrios, V. R. Almeida, R. R. Panepucci, B. S. Schmidt, and M. Lipson, “Compact silicon tunable Fabry-Perot resonator with low power consumption,” *IEEE Photon. Technol. Lett.*, vol. 16, pp. 506-508, Feb. 2004.
3. Y. Shi, C. Zhang, H. Zhang, J. H. Bechtel, L. R. Dalton, B. H. Robinson, and W. H. Steier, “Low (sub–1-volt) halfwave voltage polymeric electro-optic modulators achieved by controlling chromophore shape,” *Science*, vol. 288, pp. 119-122, April 2000.
4. T. Baehr-Jones, M. Hochberg, G. Wang, R. Lawson, Y. Liao, P. Sullivan, L. Dalton, A. Jen, and A. Scherer, “Optical modulation and detection in slotted silicon waveguides,” *Optics Express,* vol. 13, pp. 5216-5226, July 2005.
5. V. R. Almeida, Q. Xu, C. A. Barrios, and M. Lipson, “Guiding and confining light in void nanostructures,” *Optics Lett.* vol. 29, pp. 1209-1211, June 2004.
6. D. M. Kearns and R. W. Beatty, *Basic Theory of Waveguide Junctions and Introductory Microwave Network Analysis*, Pergamon Press, Oxford, London, 1967.
7. F. Payne and J. Lacey, “A theoretical analysis of scattering loss from planar optical waveguides,” *Optical and Quantum Electron.,* vol. 26, pp. 977-986, Nov. 1994.
8. IBM Photonics Research, domino.research.ibm.com/comm/research_projects.nsf/pages/photonics.fabrication.html
9. R. Legtenberg, H. Jansen, M. deBoer, and M. Elwenspoek, “Anisotropic reactive ion etching of silicon using $SF_6/O_2/CHF_3$ gas mixtures,” *J. Electrochem. Soc.*, vol. 142, pp. 2020-2028, June 1995.
10. K. Lee, D. Lim, L. Kimerling, J. Shin, and F. Cerrina, “Fabrication of ultralow-loss Si/SiO_2 waveguides by roughness reduction,” *Optics Lett.*, vol. 26, pp. 1888-1890, Dec. 2001.
11. D. Sparacin, S. Spector, and L. Kimerling, “Silicon waveguide sidewall smoothing by wet chemical oxidation,” *J. Lightwave Technol.,* vol. 23, pp. 2455-2461, August 2005.